Automatic valve plane localization in myocardial perfusion SPECT/CT by machine learning: anatomic and clinical validation

Betancur, Julian ; Rubeaux, Mathieu ; Fuchs, Tobias A ; Otaki, Yuka ; Arnson, Yoav ; Slipczuk, Leandro ; Benz, Dominik C ; Germano, Guido ; Dey, Damini ; Lin, Chih-Jen ; Berman, Daniel S ; Kaufmann, Philipp A ; Slomka, Piotr J

Abstract: Precise definition of the mitral valve plane (VP) during segmentation of the left ventricle for SPECT myocardial perfusion imaging (MPI) quantification often requires manual adjustment, which affects the quantification of perfusion. We developed a machine learning approach using support vector machines (SVM) for automatic VP placement. Methods: A total of 392 consecutive patients undergoing 99mTc-tetrofosmin stress (5 min; mean ± SD, 350 ± 54 MBq) and rest (5 min; 1,024 ± 153 MBq) fast SPECT MPI attenuation corrected (AC) by CT and same-day coronary CT angiography were studied; included in the 392 patients were 48 patients who underwent invasive coronary angiography and had no known coronary artery disease. The left ventricle was segmented with standard clinical software (quantitative perfusion SPECT) by 2 experts, adjusting the VP if needed. Two-class SVM models were computed from the expert placements with 10-fold cross validation to separate the patients used for training and those used for validation. SVM probability estimates were used to compute the best VP position. Automatic VP localizations on AC and non-AC images were compared with expert placement on coronary CT angiography. Stress and rest total perfusion deficits and detection of per-vessel obstructive stenosis by invasive coronary angiography were also compared. Results: Bland-Altman 95% confidence intervals (CIs) for VP localization by SVM and experts for AC stress images (bias, 1; 95% CI, -5 to 7 mm) and AC rest images (bias, 1; 95% CI, -7 to 10 mm) were narrower than interexpert 95% CIs for AC stress images (bias, 0; 95% CI, -8 to 8 mm) and AC rest images (bias, 0; 95% CI, -10 to 10 mm) ($P < 0.01$). Bland-Altman 95% CIs for VP localization by SVM and experts for non-AC stress images (bias, 1; 95% CI, -4 to 6 mm) and non-AC rest images (bias, 2; 95% CI, -7 to 10 mm) were similar to interexpert 95% CIs for non-AC stress images (bias, 0; 95% CI, -6 to 5 mm) and non-AC rest images (bias, -1; 95% CI, -9 to 7 mm) (P was not significant [NS]). For regional detection of obstructive stenosis, ischemic total perfusion deficit areas under the receiver operating characteristic curve for the 2 experts (AUC, 0.79 [95% CI, 0.7-0.87]; AUC, 0.81 [95% CI, 0.73-0.89]) and the SVM (0.82 [0.74-0.9]) for AC data were the same (P = NS) and were higher than those for the unadjusted VP (0.63 [0.53-0.73]) ($P < 0.01$). Similarly, for non-AC data, areas under the receiver operating characteristic curve for the experts (AUC, 0.77 [95% CI, 0.69-0.89]; AUC, 0.8 [95% CI, 0.72-0.88]) and the SVM (0.79 [0.71-0.87]) were the same (P = NS) and were higher than those for the unadjusted VP (0.65 [0.56-0.75]) ($P < 0.01$). Conclusion: Machine learning with SVM allows automatic and accurate VP localization, decreasing user dependence in SPECT MPI quantification.

DOI: https://doi.org/10.2967/jnumed.116.179911

Accepted Version

Originally published at:
Betancur, Julian; Rubeaux, Mathieu; Fuchs, Tobias A; Otaki, Yuka; Arnson, Yoav; Slipczuk, Leandro; Benz, Dominik C; Germano, Guido; Dey, Damini; Lin, Chih-Jen; Berman, Daniel S; Kaufmann, Philipp A; Slomka, Piotr J (2017). Automatic valve plane localization in myocardial perfusion SPECT/CT by machine learning: anatomic and clinical validation. Journal of Nuclear Medicine, 58(6):961-967.
DOI: https://doi.org/10.2967/jnumed.116.179911

Journal of Nuclear Medicine, published on November 3, 2016 as doi:10.2967/jnumed.116.179911

Title: Automatic Valve Plane Localization in Myocardial Perfusion SPECT/CT by Machine Learning: Anatomical and Clinical Validation

Authors: Julian Betancur[1], Mathieu Rubeaux[1], Tobias A Fuchs[2], Yuka Otaki[1], Yoav Arnson[1], Leandro Slipczuk[1], Dominik C Benz[2], Guido Germano[1], Damini Dey[1], Chih-Jen Lin[3], Daniel S Berman[1], Philipp A Kaufmann[2] and Piotr J Slomka[1]

Affiliations:

[1] Department of Imaging, Medicine, and Biomedical Sciences, Cedars-Sinai Medical Center, Los Angeles, CA, USA

[2] Department of Nuclear Medicine, Cardiac Imaging, University Hospital Zurich, Zurich, Switzerland

[3]Department of Computer Science, National Taiwan University, Taipei 106, Taiwan,

Corresponding (senior) author

Piotr Slomka, PhD, FACC

Cedars-Sinai Medical Center

8700 Beverly Boulevard, Ste. A047N

Los Angeles, California 90048

Phone: 310-423-4348

Email: Piotr.Slomka@cshs.org

First author

Julian Betancur, PhD

Postdoctoral Scientist

Cedars-Sinai Medical Center

8700 Beverly Boulevard, S. Mark Taper Building A238

Los Angeles, California 90048

Phone: 310-423-4201

Email: Julian.Betancur@cshs.org

Word count: 4987

Disclaimer:

This research was supported in part by grant R01HL089765 from the National Heart, Lung, and Blood Institute/National Institute of Health (NHLBI/NIH) (PI: PS). DB, GG and PS participate in software royalties at Cedars-Sinai Medical Center.

Short Title: Valve Localization in Cardiac SPECT

ABSTRACT

Precise definition of the mitral valve plane (VP) during segmentation of the left ventricle (LV) for single-photon emission computed tomography (SPECT) myocardial perfusion imaging (MPI) quantification often requires manual adjustment, which affects quantification of perfusion. We developed a machine learning approach using support vector machines (SVM) for automatic VP placement. **Methods:** 392 consecutive patients undergoing fast SPECT MPI ^{99m}Tc-tetrofosmin stress (5 min, 300–350 MBq)/rest (5 min, 750–1050 MBq) attenuation corrected (AC) by computed tomography (CT) and same-day coronary CT angiography (CCTA), including 48 patients with invasive angiography (ICA) and no known coronary artery disease, were studied. LV was segmented by standard clinical software (Quantitative Perfusion SPECT) by two experts, adjusting VP if needed. Two-class SVM models were computed from expert positions using 10-fold cross validation to separate the patients used for training and for validation. SVM probability estimates were used to compute the best VP position. Automatic VP localization in AC and non-AC images were compared to expert placement on CCTA. Stress and rest total perfusion deficits (TPD) and detection of per-vessel obstructive stenosis by ICA were also compared. **Results:** VP agreement (bias, 95% confidence interval) between SVM and experts was lower than inter-expert agreement for stress-AC (1, -5–7 mm) vs. (0, -8–8 mm) and rest-AC (1, -7–10 mm) vs. (0, -10–10 mm) ($p<0.01$), and similar for stress non-AC (1, -4–6 mm) vs. (0, -6–5 mm) and rest non-AC (2, -7–10 mm) vs. (-1, -9–7 mm) images (p=non-significant (NS)). For regional detection of obstructive stenosis, ischemic-TPD areas under receiver operating characteristic curve (AUCs) (95% confidence interval) of the two experts 0.79 (0.7–0.87), 0.81 (0.73–0.89) and SVM 0.82 (0.74–0.9) for AC data were the same (p=NS) and higher than for unadjusted VP 0.63 (0.53–0.73) ($p<0.01$). Similarly, for non-AC data, AUCs of experts 0.77 (0.69–0.89), 0.8 (0.72–0.88) and SVM 0.79 (0.71–0.87) were the same (p=NS) and higher than for unadjusted VP 0.65 (0.56–0.75)

($p<0.01$). **Conclusion:** Machine learning with SVM allows automatic and accurate VP localization, decreasing user-dependence in SPECT MPI quantification.

Keywords: myocardial perfusion imaging, SPECT quantification, machine learning, support vector classification, Coronary CT angiography

INTRODUCTION

Single photon emission computed tomography (SPECT) myocardial perfusion imaging (MPI) is widely used for detection and quantification of cardiac ischemia (*1*). Relative perfusion deficit quantification at stress and rest, based on total perfusion deficit (TPD) (*2*), allows quantitative estimation of ischemia. Recently, specialized cardiac SPECT scanners have dramatically improved count sensitivity and image resolution, enabling lower patient radiation doses and faster acquisitions (*3*). However, the imaging geometry and reconstruction techniques are often different from those used with the conventional Anger camera, resulting in somewhat different appearance of images (*4*) and new image artifacts (*5*). In this context, MPI software analysis packages may need to be updated for accurate quantification with the new camera systems.

Successful software-based analysis of MPI requires accurate segmentation of the left ventricular (LV) myocardium to correctly estimate myocardial perfusion deficits by comparison to normal limits. This step sometimes requires reader interaction to localize the left ventricle and the mitral valve plane (VP). From these steps, the manual adjustments of VP lead to the greatest operator intervention (*6*). We aimed to develop a novel machine learning approach for fully automated VP localization and validate it with stress and rest MPI obtained with a new generation SPECT system.

MATERIALS AND METHODS

Study Population

392 consecutive subjects undergoing hybrid computer coronary tomography angiography (CCTA), and stress/rest MPI scans on a cadmium zinc telluride SPECT camera for assessment of suspected CAD between 02/2010 and 02/2013 were considered. 350 subjects underwent both stress and rest MPI, and the remaining 42 patients underwent stress-only MPI. Invasive coronary angiography (ICA) was performed in 48/392 patients without myocardial infarction and no history

of bypass surgery. ICA cohort was used in the diagnostic validation. The study was approved by the institutional review board and the requirements to obtain informed consent was waived.

SPECT

The protocol consisted of a 1-day stress/rest MPI with standard adenosine (0.14 mg/kg/min over 6 min), or dobutamine infusion (incrementally administered, starting at 5 μg/kg/min and increasing at 1 min intervals to a maximal dose of 60 μg/kg/min until 85% of the age-predicted heart rate had been achieved), or bicycle stress. Approximately 60 min after the injection of 300–350 MBq of ^{99m}Tc-tetrofosmin, stress MPI was acquired over 5 min on Discovery NM530c scanner (GE Healthcare) equipped with a multipinhole collimator and 19 cadmium zinc telluride detectors (*7*). This was followed by acquisition of rest MPI several minutes after administration of 750–1050 MBq ^{99m}Tc-tetrofosmin (*5,8*). Attenuation correction was performed on stress and rest images with a low-dose 64-slice CT scan acquired with prospective electrocardiography triggering (*9,10*). Cadmium zinc telluride images were reconstructed on a dedicated Xeleris workstation (GE Healthcare) by an optimized iterative reconstruction algorithm with maximum likelihood expectation maximization (*8*), as used in the clinical routine.

SPECT Quantitative Analysis

Attenuation corrected (AC) and non-AC MPI images were processed using standard clinical software (Quantitative Perfusion SPECT; Cedars-Sinai Medical Center) (*11*). LV contours were verified independently on stress and rest images by two experienced observers (Expert 1, Expert 2), both nuclear medicine technologists with > 15 years of dedicated experience in nuclear cardiology. Experts were blinded to any of the clinical results. When needed, they corrected the gross initial LV localization, the LV mask (region containing left ventricle) and adjusted the VP position. Stress and rest TPD (*2*), and per-vessel TPD for the coronary vessels territories were

obtained (*2*). To avoid ambiguity during machine learning training, the inter-observer normal/abnormal discrepancies of global TPD measures (at threshold 5%) due to VP positioning were resolved by a third experienced observer (imaging cardiologist) blinded to previous results.

CCTA

CCTA images were acquired on a 64-slice CT system (Lightspeed VCT or Discovery HD750; GE Healthcare) (*12,13*). A contrast-enhanced prospective electrocardiography triggered CCTA was acquired with inspiration breath-hold at 75% if the R-R interval as previously reported (*12*). Metoprolol was administrated intravenously before the examination if heart rate was greater than 65 beat/min and 2.5 mg of isosorbide dinitrate was administrated sublingually to obtain optimal image quality. Iodixanol (Visipaque 320; 320 mg/mL; GE Healthcare) was injected into an antecubital vein followed by 50 mL of saline solution via an 18-gauge catheter. Contrast media volume (40–105 mL) and flow rate (3.5–5 mL/s) were adapted to body surface area (*9*).

CCTA Analysis

CCTA was used only as the anatomical reference for the evaluation of the algorithm and was not used by the machine learning algorithm. The distance from the endocardial surface of the apex to the anatomical VP centroid was defined by two additional experienced observers, different from Experts 1 and 2, in the vertical and the horizontal long-axis orientations (Fig. 1). During CCTA measurements, the readers were blinded to the SPECT measurements. The mean of the two values for each observation (horizontal and vertical long axis) was used for the comparison to the corresponding apex-VP distance obtained from MPI images.

ICA

ICA through the femoral or radial artery was performed in an experienced catheterization laboratory (University Hospital Zurich) following the clinical protocol, which consists of a biplane angiography of the left coronary artery in four orientations and of the right coronary artery in two orientations. Each vessel was visually scored as being normal or stenosed by an experienced interventional cardiologist reflecting daily clinical routine in the catheterization laboratory. Obstructive stenosis was defined as a diameter reduction of > 70%.

Machine Learning: Overview

Experts 1 and 2 localized VP in SPECT images by their inferred knowledge of the heart anatomy. The proposed machine learning approach encapsulates this knowledge and estimates the VP position by a two-class model that enables a continuous estimation of VP correct position probability. This approach requires the definition of correct and incorrect VP positions based on the distance from expert placement (Fig. 2). VP positions defined by both experts were used as examples of "correct" positions while "incorrect" positions were generated at every 2.5 mm along the LV long axis, between 50 mm and 150 mm from the apex (Fig. 2), to reflect anatomical constraints. Thus, 784 correct positions (392 images, 2 experts) for the stress images and 700 for the rest images were generated. In addition, 6 to 40 incorrect positions were generated for each image.

Machine Learning: Feature Selection

In total, 22 heuristically derived features related to the VP position computed from intensity, shape and patient gender were included in the search for the best features performed during the system training. Intensity attributes included the values of raw intensity as well as individual extent and TPD values in the basal segments. Shape attributes included myocardial mass and VP contour perimeter. Previously proposed VP and gross LV shape failure indicators were also considered (*6*). LV segmentation of gated images have demonstrated to outperform ungated

segmentation (*6*); thus, the ungated-to-gated VP distance and the differences in myocardial masses were also included. Attributes obtained from gated studies were included only if the segmentation quality control flag indicated correct segmentation (*6*) without any manual adjustment of gated studies. These features were evaluated for their incremental value in deciding if the VP was "correctly" placed on MPI. We ranked the attributes following the information gain as in our previous work (*14*), and selected the top-ranked attributes with gain > 0 that also monotonically increased the area under receiver operating characteristic curve (AUC).

Machine Learning: Support Vector Classification

Automatic VP localization is achieved by finding the position with the highest probability of being correct. We used a two-class Support Vector Machines (SVM) classification approach (*15*) that automatically estimates the VP position and its probability from a set of potential positions sampled by 1 mm between the limit bounds defined above (Fig. 2). The radial basis function SVM model, defined by the regularization parameter (C) and kernel parameter (gamma), was selected. The two classes defined are "Correct VP" position and "Incorrect VP" position. The number of correct and incorrect samples were balanced during training by penalty weighting (*15*).

Machine learning: 10-fold Cross Validation

The separation of training and testing data was achieved using a nested 10-fold cross validation procedure. The main advantages of this procedure are that it reduces the variance in prediction error leading to a more accurate estimate of model performance, maximizes the use of data for training and validation without overfitting or overlap between test and validation data, and guards against testing hypotheses suggested by arbitrarily split data (*16*). The procedure divided the study population into 10 non-overlapping groups of patients of approximately the same size (*17*). 10 folds were built, with each group used in turn as validation set, and the remaining 9 groups as

training set. 10 models are then trained and validated using these folds. The validation results are then stacked to provide the overall performance. The SVM C and gamma parameters were computed inside the folds by a standard grid search procedure (*17*).

Anatomical Validation

The anatomical validation included comparisons of VP positions obtained by the two experts and the automatic VP localization by SVM, and against the position of the anatomical mitral VP in CCTA. When comparing to CCTA, half of the distance between the end-diastolic and the end-systolic VP was added to the VP position to correct for expected difference between VP position for ungated MPI and mitral VP positions in CCTA from the 70% diastolic phase. In addition, a comparison of the transient ischemic dilation ratio (*18*) estimated by the two experts and the SVM was also performed.

Diagnostic Validation

Prediction of obstructive stenosis by ICA in the coronary vessels territories by per-vessel ischemic-TPD and stress-TPD was used to evaluate diagnostic accuracy after VP localization. The prediction before manual VP adjustment by experts (Unadjusted) has also been provided for reference.

Statistical Analysis:

Bland-Altman difference plots (*19*) depicting bias and agreement limits (95% confidence interval [95% CI]) were used to assess agreement in VP positions, transient ischemic dilation ratio and TPD. Paired Wilcoxon test was used to evaluate differences in bias. Levene's homogeneity of variance test was used to assess differences in 95% CI. Pearson correlation and differences between paired correlations were also computed (*20*). Paired DeLong test was used to evaluate difference

between AUCs (*21*). Two-sided p-values < 0.05 were considered as significant. All statistical analysis were implemented in R programming language version 3.2.3 (*22*).

RESULTS

Patients

Clinical characteristics of the population are shown in Table 1. All subjects underwent SPECT MPI and CCTA acquisition. For the CCTA analysis, 18 stress and 16 rest images were rejected because the apex could not be observed on CCTA (11 cases) and because studies were of poor quality (7 cases). This resulted in 374 stress studies and 334 rest studies retained for the validation of VP positions against CCTA.

Of the 48 patients with ICA correlations and no myocardial infarction (144 territories), 34% (49/144) vessels had obstructive stenosis distributed in 22 left anterior descending, 13 left circumflex and 14 right coronary artery territories.

VP Positioning on SPECT MPI

For stress images, the VP position by the standard software was adjusted in 38% AC (149/392) and 18.6% non-AC (73/392) cases by Expert 1 and in 44.4% AC (174/392) and 21.2% non-AC (83/392) cases by Expert 2. For rest images, the VP was adjusted in 64.9% AC (227/350) and 61.4% non-AC (215/350) and in 65.4% AC (229/350) and 63.7% non-AC (223/350) cases, respectively. VP positions in 6.9% AC (27/392), 5.1% non-AC (20/392) stress and 13.7% AC (48/350), 8.3% non-AC (29/350) rest images were reviewed by a third expert to solve the diagnostic discrepancies between Experts 1 and 2 for SVM model training.

Feature Selection

Six attributes were selected during the feature selection step for AC images and eight for non-AC images (Table 2, Supplemental Fig. 1). Noteworthy, both previously proposed quality control indicators (*6*) were selected for AC and non-AC images.

Anatomical Validation

The differences between VP positions on CCTA and VP positions on MPI for Expert 1, Expert 2 and SVM had similar 95% CI (Fig. 3). High correlation between the two experts (AC: $r = 0.79$, non-AC: $r = 0.90$) was observed for stress images. For stress images, SVM-Expert 2 correlation (AC: $r = 0.87$, non-AC: $r = 0.86$) was greater for AC but lower for non-AC images compared to SVM-Expert 1 correlations (AC: $r = 0.78$, non-AC $r = 0.92$) ($p < 0.001$). For rest AC images, similar (p=non significant (NS) for comparison) correlations were found between Experts 1 and 2 ($r = 0.72$), SVM and Expert 1 ($r = 0.68$), SVM and Expert 2 ($r = 0.69$). For rest non-AC images, Expert 1-Expert 2 ($r = 0.80$) and SVM-Expert 1 ($r = 0.73$) correlations were higher than SVM-Expert 2 ($r = 0.66$) correlation ($p < 0.01$).

The 95% CI of VP positions between SVM and experts were lower for AC and similar for non-AC images than those between experts (Fig. 4). For stress images, similar bias was observed between SVM and experts, and between experts (p = NS) while rest-AC and stress/rest non-AC bias was higher for SVM ($p < 0.05$). The 95% CI was the same for SVM and experts when compared to compared to CCTA (Supplemental Fig. 2).

For transient ischemic dilation ratio, lower bias and lower 95% CI were found between SVM and experts than between the two experts (Fig. 5). Significant AC and non-AC transient ischemic dilation ratio correlation was found between the two experts (AC: $r = 0.65$, non-AC: $r = 0.72$), SVM and Expert 1 (AC: $r = 0.67$, non-AC: $r = 0.88$), SVM and Expert 2 (AC: $r = 0.82$, non-

AC: r = 0.66). SVM correlation with Expert 2 was higher for AC but lower for non-AC images than with Expert 1 ($p < 0.001$).

Diagnostic Validation

Global TPD bias between SVM and experts was similar to that between the two experts (Fig. 6). High AC and non-AC correlation was found for global stress-TPD and rest-TPD by the two experts (stress AC: r = 0.96, stress non-AC: r = 0.98) (rest AC: r = 0.97, rest non-AC: r = 0.92), SVM and Expert 1 (r = 0.96, r = 0.97) (r = 0.96, r = 0.86), SVM and Expert 2 (r = 0.97, r = 0.98) (r = 0.97, r = 0.87). SVM correlation with Expert 2 was higher than with Expert 1 ($p < 0.001$).

AUC (95% CI) for the per-vessel detection of obstructive stenosis by regional ischemic-TPD (Fig. 7) and stress-TPD (Supplemental Fig. 3) for the two experts and SVM was similar (p = NS) and higher than for unadjusted VP.

DISCUSSION

We propose a novel method for automatic VP localization in MPI images. The machine learning approach allows us to encapsulate expert knowledge and capture the complex pattern changes caused by VP variations using an optimal combination of high level image features. This can be difficult to accomplish by traditional image processing approaches. The SVM model combines features such as intensity, shape and information from gated images to find the most likely VP position on MPI. The validation was performed in a rigorous fashion using nested 10-fold cross validation. Therefore, only patients unseen by the algorithm were used in the validation avoiding possible bias.

VP adjustment is the only explicitly-defined (without further algorithm override) adjustment by the user in the majority of software packages. This adjustment is subjective and time

consuming; consequently, it is the major contributor to the inter-observer variability of quantitative perfusion parameters (*6*). Xu et al. have previously proposed two quality control indicators of myocardial segmentation quality, one indicating VP failure (*6*). However, while the detection of gross shape failures in the LV segmentation algorithm was excellent, the detection of VP failures was less optimal. Indeed, this variability could lead to the potential degradation of the diagnostic accuracy of MPI in the hands of inexperienced users. Incorrect VP localization leads to inaccurate definition of the LV base and a consequent flawed polar-map subdivision of the myocardial segments. TPD computation relies on the comparison of normalized local intensity counts to corresponding local normal limits (*2*). Thus, precise VP placement is required to avoid the polar map localization mismatch when comparing to normal limits.

The automatic VP positioning was evaluated using CCTA as the anatomical reference standard and ICA as the diagnostic reference standard. The results show that automated VP localization performs as well as experts, and results in similar diagnostic accuracy. Therefore, our results suggest that the algorithms trained by expert annotations could be deployed to entirely eliminate manual adjustment of VP in MPI, thus significantly decreasing quantification subjectivity and facilitating the optimal perfusion quantification for less experienced readers.

Although major efforts to standardize MPI analysis (*23*–*26*) have been reported, current recommended method for MPI interpretation is still based on time consuming and subjective visual scoring of regional perfusion tracer uptake (*27*). Automatic quantification of MPI would reduce this subjectivity, but current techniques still require the user to make manual adjustments. In our study, two highly experienced observers corrected VP failures in substantial number of MPI studies. We have shown here that without this user correction the diagnostic accuracy of MPI is significantly degraded. By applying the machine learning approach, we were able to totally automate the VP selection.

This study has some limitations. First, it is limited to the localization of the VP center which is the only adjustment performed in current clinical routine. Second, it is a single-center study using a one-vendor camera. However, the methodology proposed here can be applied to other systems. Further tests for conventional camera images with available CCTA correlations should be performed. Third, for anatomical validation we relied on CCTA measurements which provides excellent anatomical information but has limitations due to phase matching with ungated MPI images that may have contributed to the systematic bias of the CCTA comparisons. Finally, the angiographic validation was available only in a subset of the overall population.

CONCLUSION

We have demonstrated that a machine learning approach allows full automation of valve plane localization in MPI acquired by the new generation SPECT cameras. This approach represents an important step in efforts to allow objective quantification of MPI, without need for expert intervention due to contour correction.

DISCLOSURE

This research was supported in part by grant R01HL089765 from the National Heart, Lung, and Blood Institute/National Institute of Health (NHLBI/NIH) (PI: PS). DB, GG and PS participate in software royalties at Cedars-Sinai Medical Center.

ACKNOWLEDGMENTS

We thank Joanna Liang for the proof reading of this paper.

REFERENCES

1. Einstein AJ. Effects of radiation exposure from cardiac imaging: how good are the data? *J Am Coll Cardiol.* 2012;59:553–565.
2. Slomka PJ, Nishina H, Berman DS, et al. Automated quantification of myocardial perfusion SPECT using simplified normal limits. *J Nucl Cardiol.* 2005;12:66–77.
3. Slomka PJ, Patton JA, Berman DS, Germano G. Advances in technical aspects of myocardial perfusion SPECT imaging. *J Nucl Cardiol.* 2009;16:255–276.
4. Sharir T, Ben-Haim S, Merzon K, et al. High-speed myocardial perfusion imaging initial clinical comparison with conventional dual detector anger camera imaging. *JACC Cardiovasc Imaging.* 2008;1:156–263.
5. Fiechter M, Ghadri JR, Kuest SM, et al. Nuclear myocardial perfusion imaging with a novel cadmium-zinc-telluride detector SPECT/CT device: first validation versus invasive coronary angiography. *Eur J Nucl Med Mol Imaging.* 2011;38:2025–2030.
6. Xu Y, Kavanagh P, Fish M, et al. Automated quality control for segmentation of myocardial perfusion SPECT. *J Nucl Med.* 2009;50:1418–1426.
7. Herzog BA, Buechel RR, Katz R, et al. Nuclear myocardial perfusion imaging with a cadmium-zinc-telluride detector technique: optimized protocol for scan time reduction. *J Nucl Med.* 2010;51:46–51.
8. Buechel RR, Herzog BA, Husmann L, et al. Ultrafast nuclear myocardial perfusion imaging on a new gamma camera with semiconductor detector technique: first clinical validation. *Eur J Nucl Med Mol Imaging.* 2010;37:773–778.

9. Pazhenkottil AP, Husmann L, Buechel RR, et al. Validation of a new contrast material protocol adapted to body surface area for optimized low-dose CT coronary angiography with prospective ECG-triggering. *Int J Cardiovasc Imaging*. 2010;26:591–597.

10. Fiechter M, Ghadri JR, Wolfrum M, et al. Downstream resource utilization following hybrid cardiac imaging with an integrated cadmium-zinc-telluride/64-slice CT device. *Eur J Nucl Med Mol Imaging*. 2012;39:430–436.

11. Germano G, Kavanagh PB, Waechter P, et al. A new algorithm for the quantitation of myocardial perfusion SPECT. I: technical principles and reproducibility. *J Nucl Med.* 2000;41:712–719.

12. Husmann L, Valenta I, Gaemperli O, et al. Feasibility of low-dose coronary CT angiography: first experience with prospective ECG-gating. *Eur Heart J*. 2008;29:191–197.

13. Fuchs TA, Stehli J, Fiechter M, et al. First experience with monochromatic coronary computed tomography angiography from a 64-slice CT scanner with Gemstone Spectral Imaging (GSI). *J Cardiovasc Comput Tomogr.* 2013;7:25–31.

14. Arsanjani R, Dey D, Khachatryan T, et al. Prediction of revascularization after myocardial perfusion SPECT by machine learning in a large population. *J Nucl Cardiol.* 2014;22:877–884.

15. Chang C-C, Lin C-J. LIBSVM: A library for support vector machines. *ACM Trans Intell Syst Technol.* 2011;2:1–27.

16. Molinaro AM., Simon R., Pfeiffer RM. Prediction error estimation: a comparison of resampling methods. *Bioinformatics.* 2005;21:3301–3307.

17. Hsu C-W, Chang C-C, Lin C-J. A practical guide to support vector classification. Department of Computer Science: National Taiwan University; 2003.

18. McLaughlin MG, Danias PG. Transient ischemic dilation: a powerful diagnostic and prognostic finding of stress myocardial perfusion imaging. *J Nucl Cardiol.* 2002;9:663–667.

19. Martin Bland J, Altman D. Statistical methods for assessing agreement between two methods of clinical measurement. *The Lancet.* 1986;327:307–310.

20. Revelle W. psych: Procedures for psychological, psychometric, and personality research. Evanston, Illinois: Northwestern University; 2015.

21. Robin X, Turck N, Hainard A, et al. pROC: an open-source package for R and S+ to analyze and compare ROC curves. *BMC Bioinformatics.* 2011;12:77.

22. Team RC. A language and environment for statistical computing. Vienna, Austria: R Foundation for Statistical Computing; 2015.

23. Germano G, Kavanagh PB, Slomka PJ, Van Kriekinge SD, Pollard G, Berman DS. Quantitation in gated perfusion SPECT imaging: the Cedars-Sinai approach. *J Nucl Cardiol.* 2007;14:433–454.

24. Garcia EV, Faber TL, Cooke CD, Folks RD, Chen J, Santana C. The increasing role of quantification in clinical nuclear cardiology: the Emory approach. *J Nucl Cardiol.* 2007;14:420–432.

25. Ficaro EP, Lee BC, Kritzman JN, Corbett JR. Corridor4DM: the Michigan method for quantitative nuclear cardiology. *J Nucl Cardiol.* 2007;14:455–465.

26. Liu Y. Quantification of nuclear cardiac images: the Yale approach. *J Nucl Cardiol.* 2007;14:483–491.

27. Xu Y, Hayes S, Ali I, et al. Automatic and visual reproducibility of perfusion and function measures for myocardial perfusion SPECT. *J Nucl Cardiol.* 2010;17:1050–1057.

FIGURE LEGENDS

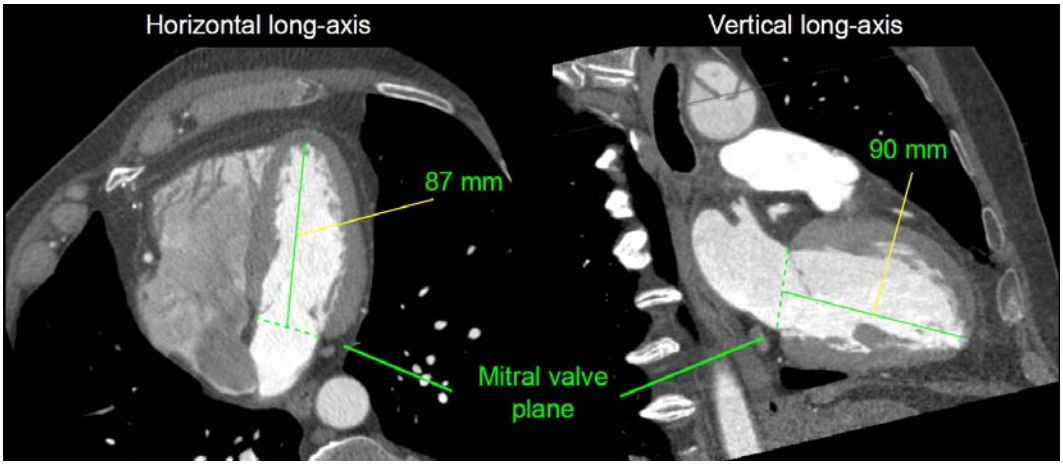

FIGURE 1. Example of mitral valve plane localization in contrast-enhanced coronary computed tomography angiography. Inner left ventricular length measured from the apex in the endocardial wall to the blood-pool centroid in the valve plane was measured in horizontal and vertical long-axis views from ungated stress MPI images. The average value (88.5 mm) was obtained for this subject.

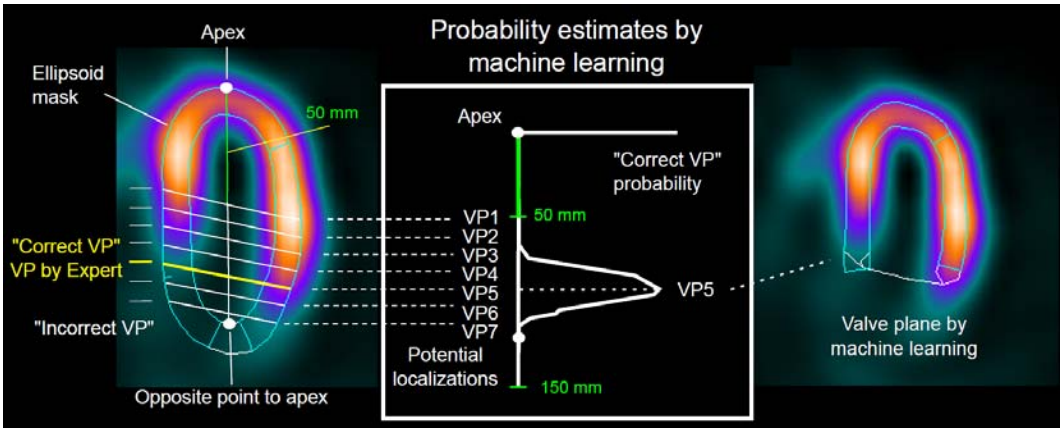

FIGURE 2. Machine learning localization of the valve plane (VP) in MPI images. A two-class SVM model trained from VP positions verified by two experts is used to estimate the most likely VP localization in the left ventricle. SVM: support vector machines.

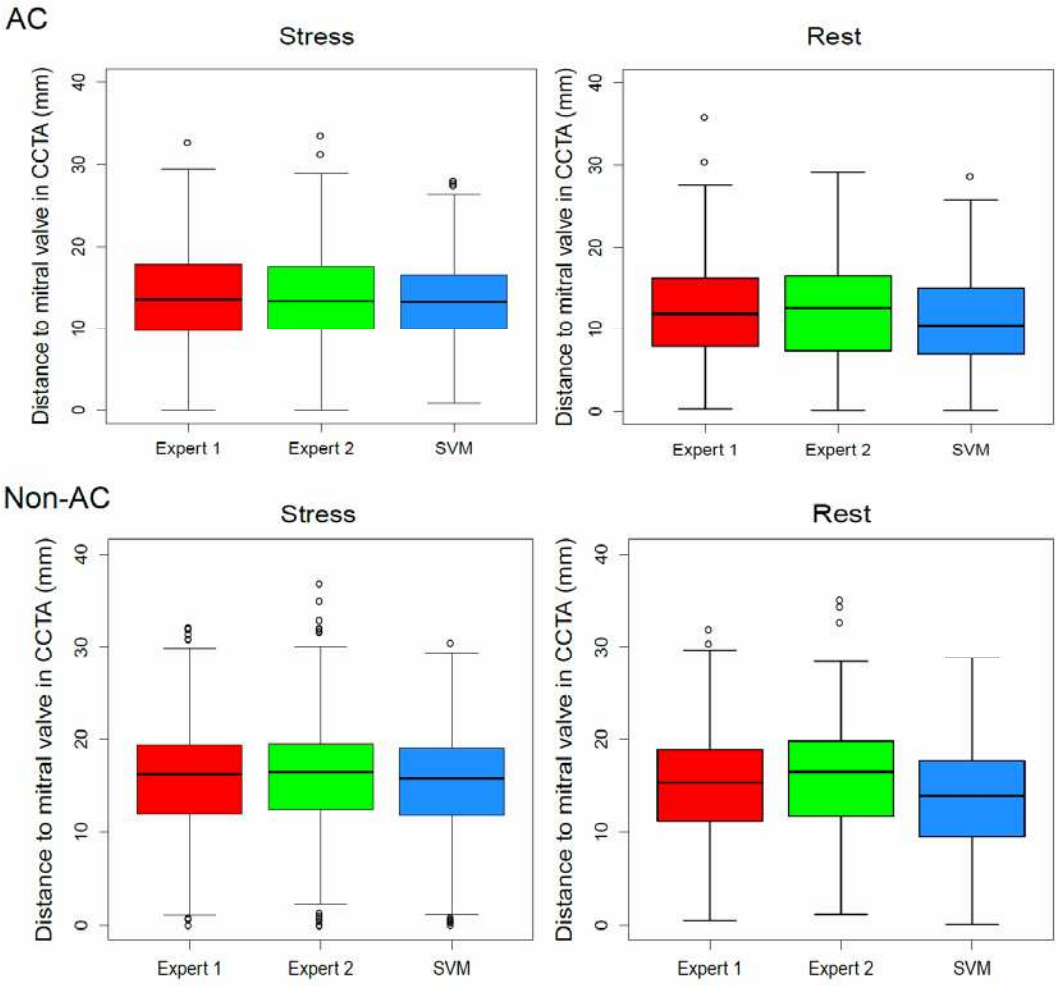

FIGURE 3. Distance to the valve plane (VP) in CCTA. Boxplots for the distance to CCTA VP position for VP positions in stress and rest MPI AC/non-AC images from two experts (red, green) and the automatic SVM procedure (blue). Similar stress and rest 95%CI were found for Expert 1, Expert 2 and SVM (p = NS). AC: attenuation corrected, CCTA: coronary computed tomography angiography, CI: confidence interval, SVM: support vector machines.

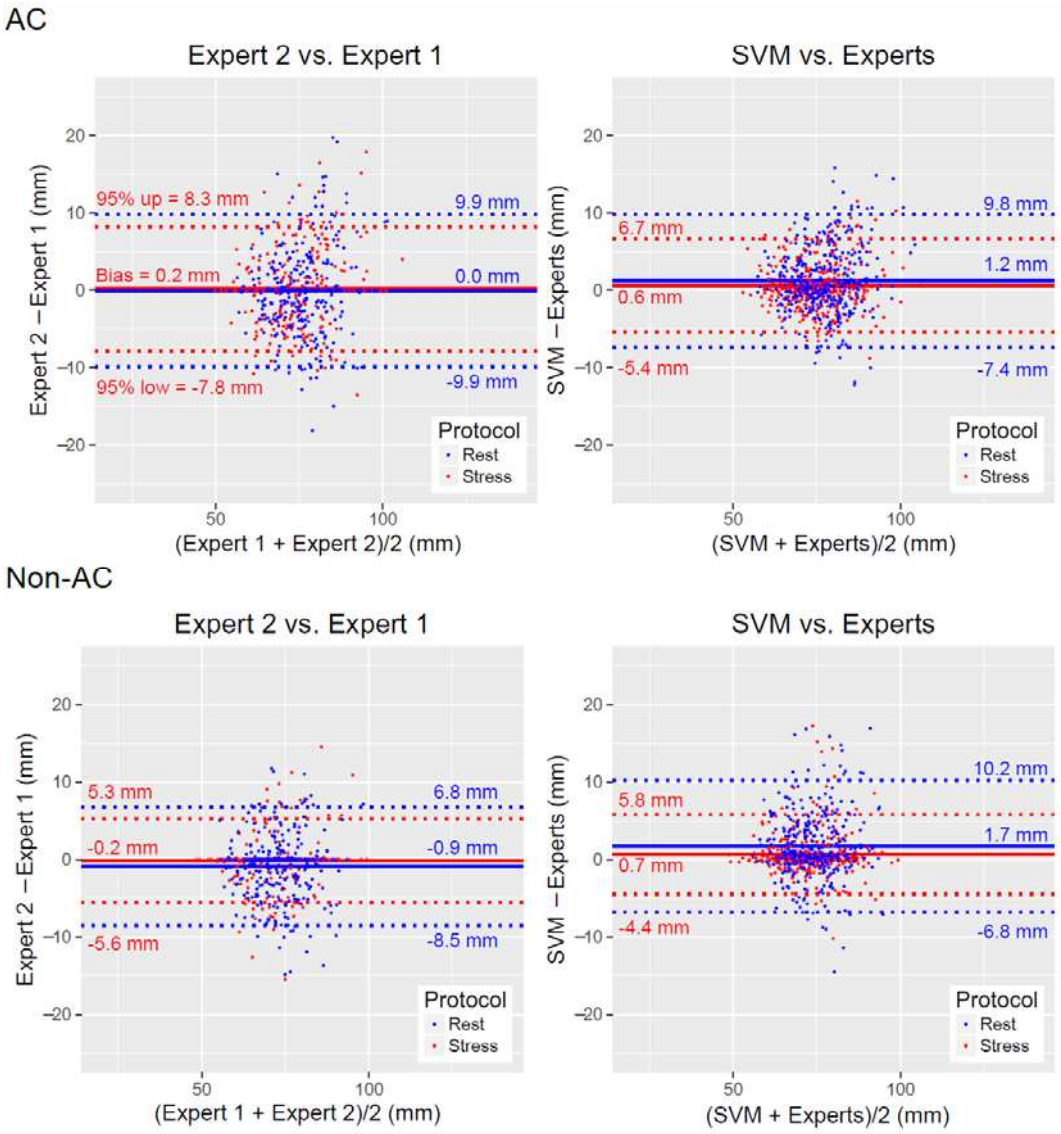

FIGURE 4. Valve plane (VP) localization agreement. Bland-Altman difference plots showing the distance from the apex to the VP center in stress (red) and rest (blue) images using VP positions from two experts and the automatic VP localization procedure (SVM). Agreement for experts (Expert 1 vs. Expert 2) and SVM with average VP positions from experts (Experts = (Expert 1 + Expert 2)/2) had lower 95% CI for stress/rest AC ($p < 0.01$) and the same for stress/rest non-AC

images (p = NS). AC: attenuation corrected, CI: confidence interval, SVM: support vector machines.

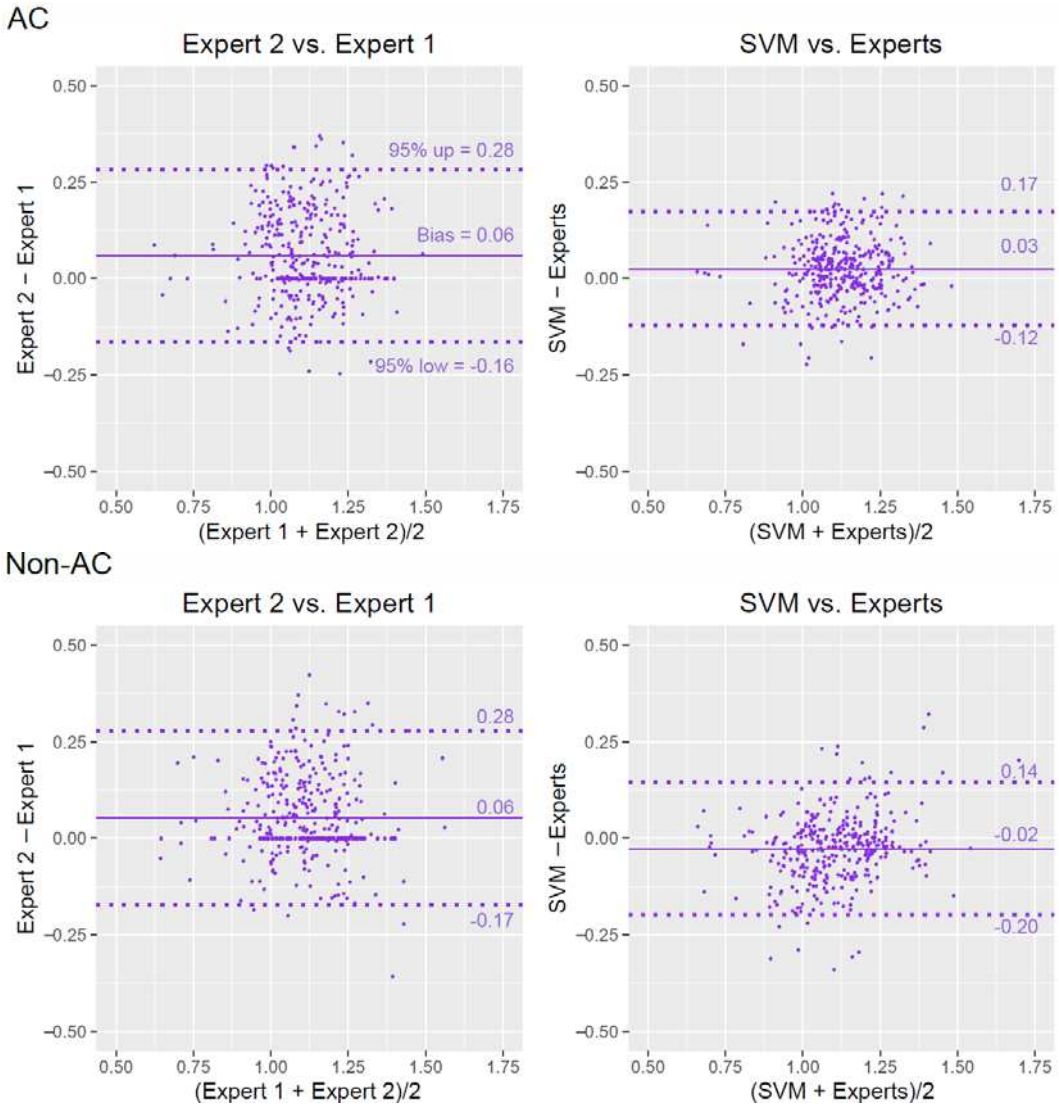

FIGURE 5. TID agreement. Bland-Altman difference plots showing TID for VP positions from two experts and the automatic VP localization procedure (SVM) in stress and rest AC/non-AC images. TID average from experts (Experts = (Expert 1 + Expert 2)/2) is used as reference for the SVM plot. Lower bias and lower 95% CI were found for SVM vs. Experts ($p < 0.001$). AC: attenuation corrected, CI: confidence interval, TID: transient ischemic dilation ratio, SVM: support vector machines, VP: valve plane.

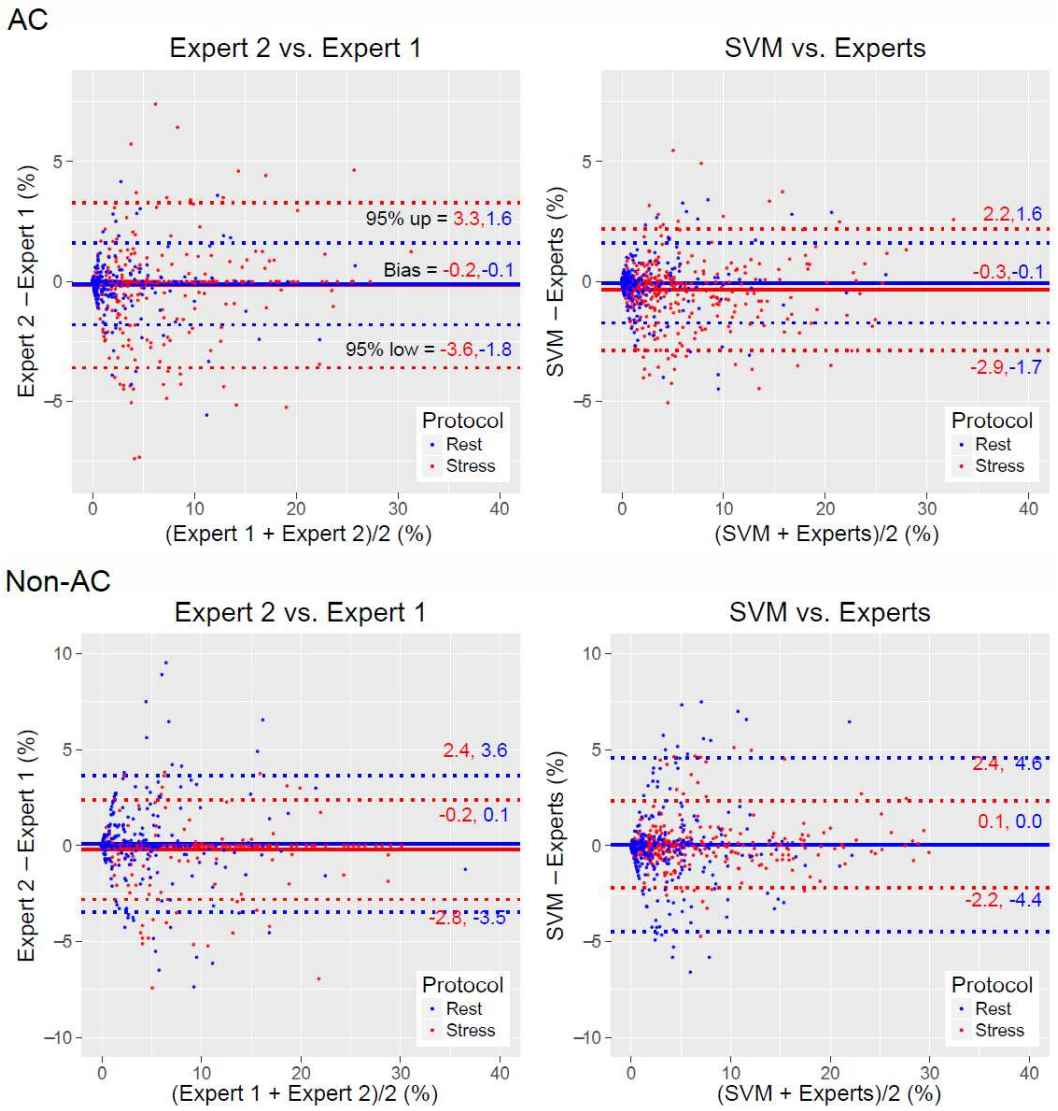

FIGURE 6. TPD agreement. Bland-Altman difference plots showing global stress-TPD (red) and rest-TPD (blue) for valve plane (VP) positions from two experts and the automatic VP localization procedure (SVM). TPD average from experts (Experts = (Expert 1 + Expert 2)/2) is used as reference for the SVM plot. Similar stress and rest bias and rest 95% CI were found for AC and non-AC images ($p = NS$). Higher 95% CI was found for SVM vs. Experts ($p < 0.05$). AC: attenuation corrected, SVM: support vector machines, TPD: total perfusion deficit.

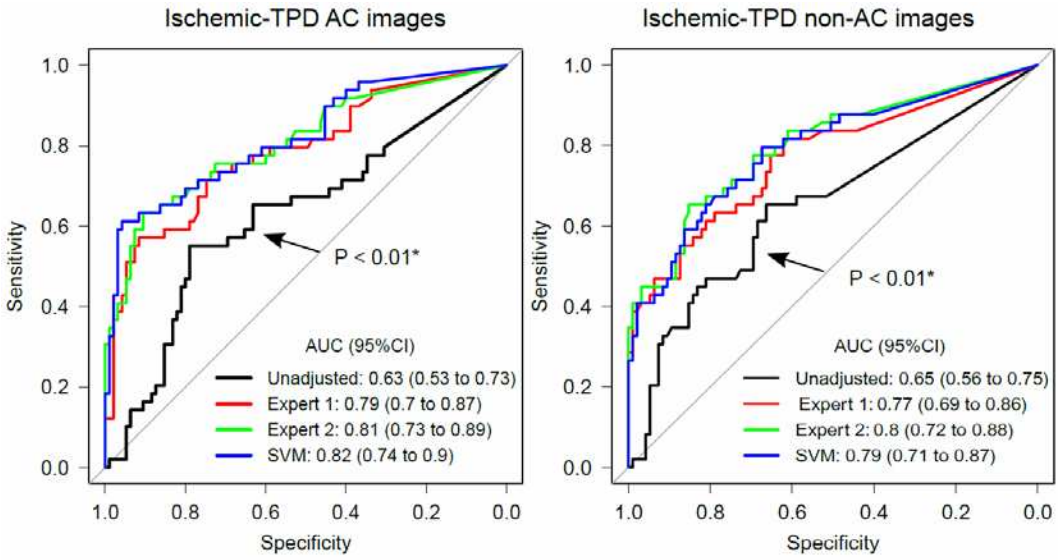

FIGURE 7. Diagnostic outcome agreement. Prediction of per-vessel obstructive stenosis from ICA by ischemic-TPD (stress-rest) computed from non-adjusted VP positions (Unadjusted), valve plane (VP) positions from two experts and the automatic VP localization procedure (SVM). AC: attenuation corrected, ICA: invasive coronary angiography, AUC: area under receiver operating characteristic curve, SVM: support vector machines, TPD: total perfusion defect. (*) AUC lower than for Expert 1, Expert 2 or SVM. All other comparisons not significant (p = NS).

TABLE 1. Population characteristics.

Characteristic	ALL (n = 392)	MALE (n = 279)	FEMALE (n = 113)
Age (years)	62.5 ± 9.9	61.9 ± 10	64 ± 9.4
BMI (kg/m2)	27.5 ± 4.9	27.6 ± 4.5	27.1 ± 5.9
Obesity (BMI >30 kg/m2), n (%)	100 (26)	69 (25)	31 (27)
Previous cardiac events, n (%):			
Myocardial infarction	64 (16)	56 (20)	8 (7)
PCI	58 (15)	51 (18)	7 (6)
CABG	33 (9)	30 (11)	3 (3)

Continuous variables are reported as mean ± standard deviation. BMI: body-mass index; PCI: percutaneous coronary intervention; CABG: coronary artery bypass grafting.

TABLE 2. Selected attributes during support vector machines model training.

Type	Images (AC/non-AC/both)	**Attribute**
Intensity	Both	QC for VP failure (*6*)
	Both	Sum of basal counts normalized to the maximum segment (%)
	Rest non-AC	Sum of basal counts normalized to background (%)
Shape	Both	QC for gross LV contour failure (*6*)
	Both	Normalized perimeter of the VP contour (%)
	Non-AC	VP contour perimeter (mm)
	Stress non-AC	Myocardial mass (gr)
Data from gated scan	Both	Distance to VP in gated image (mm)
	Both	Ungated-to-gated difference of myocardial mass (gr)

AC: attenuation corrected, QC: quality control, VP: valve plane

SUPPLEMENTAL FIGURE 1. Feature selection for AC/non-AC stress/rest images. Selected attributes are shown in red. AC: attenuation corrected, TPD: total perfusion deficit, VP: valve plane, VP QC: valve plane quality control indicator, Shape QC: left ventricular contour quality control flag. (†) Area under the receiver operating characteristic curve for the prediction of "correct VP". (*) Normalized to the radius of the left ventricular contour. (**) Normalized to corresponding measure for background.

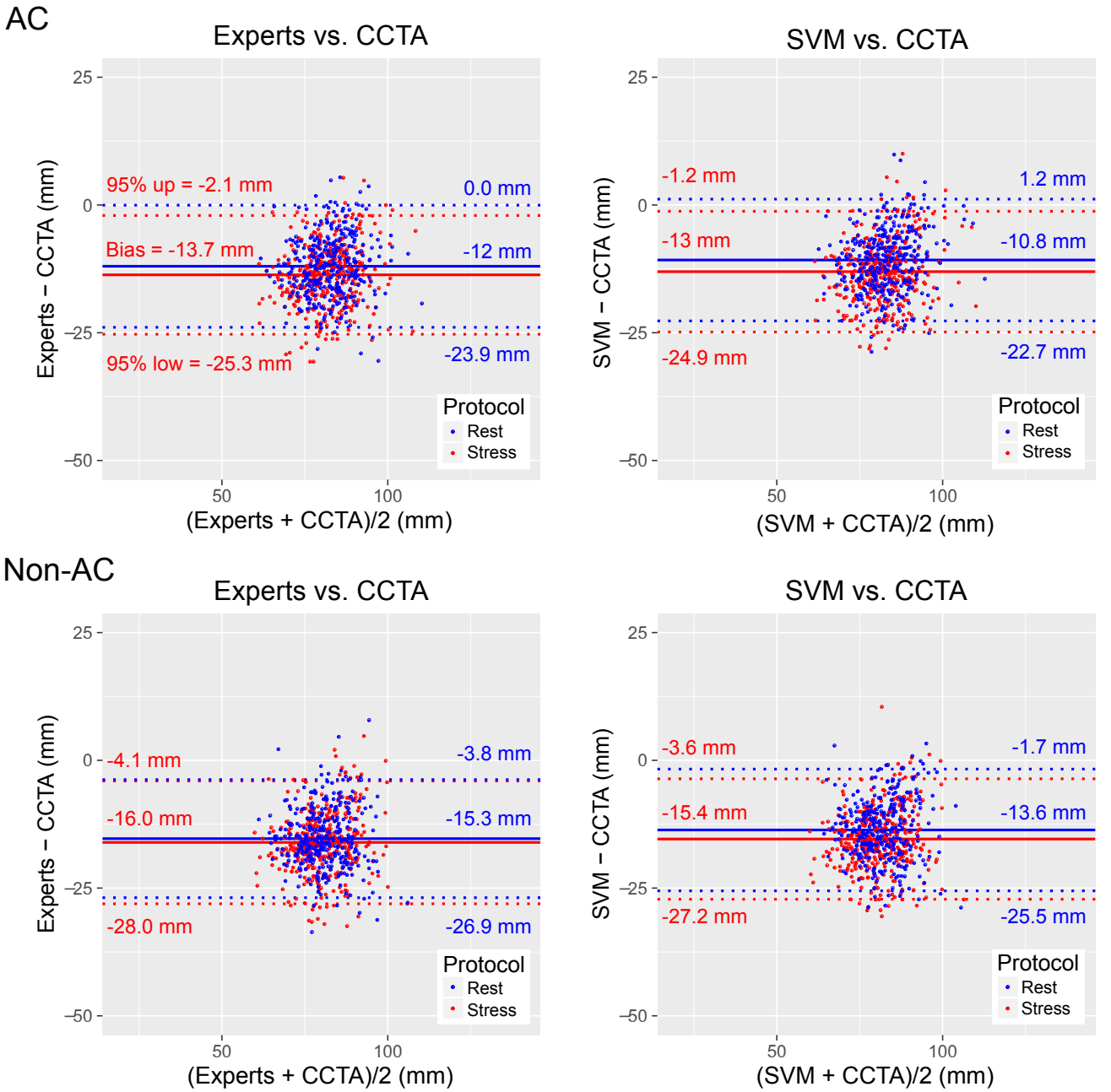

SUPPLEMENTAL FIGURE 2. Valve plane (VP) localization agreement. Bland-Altman difference plots showing the distance from the apex to the VP center in stress (red) and rest (blue) using the average VP positions from the two experts (Experts = (Expert 1 + Expert 2)/2), the automatic VP localization procedure (SVM) and CCTA positions of the mitral valve. Agreement of Experts and SVM with the mitral valve from CCTA had similar stress and rest 95% CI for AC and non-AC images (p = NS). AC: attenuation corrected, CCTA: coronary computed tomography angiography, CI: confidence interval, SVM: support vector machines.

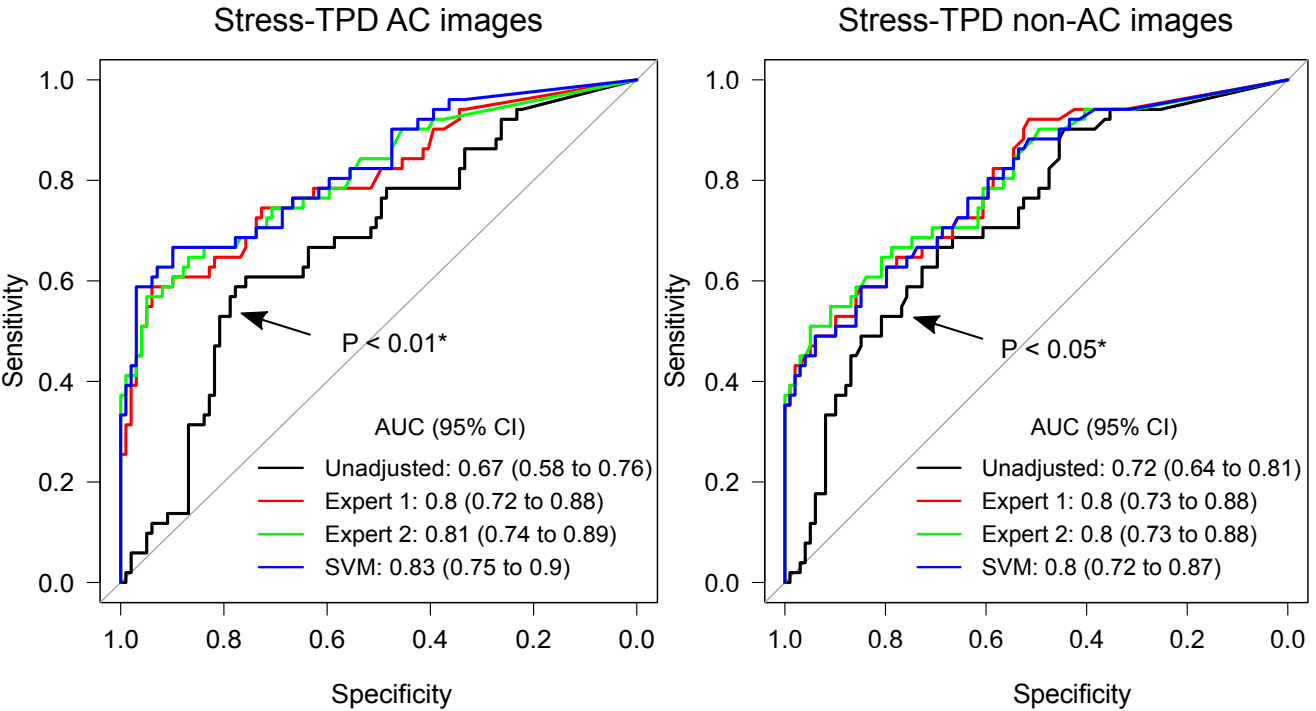

SUPPLEMENTAL FIGURE 3. Diagnostic outcome agreement. Prediction of per-vessel obstructive stenosis from ICA by stress-TPD computed from non-adjusted valve plane (VP) positions (Unadjusted), VP positions from two experts and the automatic VP localization procedure (SVM). ICA: invasive coronary angiography, AC: attenuation corrected, AUC: area under receiver operating characteristic curve, SVM: support vector machines, TPD: total perfusion deficit. (*) AUC lower than for Expert 1, Expert 2 or SVM. All other comparison not significant (p=NS).

The Journal of NUCLEAR MEDICINE

Automatic Valve Plane Localization in Myocardial Perfusion SPECT/CT by Machine Learning: Anatomical and Clinical Validation

Julian Betancur, Mathieu Rubeaux, Tobias Fuchs, Yuka Otaki, Yoav Arnson, Leandro Slipczuk, Dominik Benz, Guido Germano, Damini Dey, Chih-Jen Lin, Daniel Berman, Philipp Kaufmann and Piotr Slomka

J Nucl Med.
Published online: November 3, 2016.
Doi: 10.2967/jnumed.116.179911

The Journal of Nuclear Medicine is published monthly.
SNMMI | Society of Nuclear Medicine and Molecular Imaging
1850 Samuel Morse Drive, Reston, VA 20190.
(Print ISSN: 0161-5505, Online ISSN: 2159-662X)

SNMMI SOCIETY OF NUCLEAR MEDICINE AND MOLECULAR IMAGING